2016

Experimental and Numerical Study of a Mobile Reversible Air Conditioning-Heat Pump System

Lili Feng
University of Illinois at Urbana-Champaign, United States of America, lfeng8@illinois.edu

Pega Hrnjak
University of Illinois at Urbana-Champaign, United States of America, pega@illinois.edu

Experimental and Numerical Study of a Mobile Reversible Air Conditioning-Heat Pump System

Lili FENG[1*], Pega HRNJAK[1,2]

[1]Department of Mechanical Science and Engineering,
University of Illinois at Urbana-Champaign
Urbana, IL, USA
lfeng8@illinois.edu
[2]Creative Thermal Solution,
Urbana, IL, USA
pega@illinois.edu
* Corresponding Author

ABSTRACT

Electric vehicles suffer from 'range anxiety', while traditional resistive heating consumes a lot of electric energy and further reduces EV drive range largely. Mobile reversible air conditioning-heat pump system is an energy efficient way of providing heat to EV cabin climate. In this paper, an AC/HP system based on the Nissan Leaf system configuration was studied experimentally and numerically. This system consists of three heat exchangers, an open-shaft compressor, two expansion valves, and two flow control valves. A system model was built, heating performance characteristics were investigated under various operating conditions, and were compared to experimental findings. Refrigerant charge imbalance when switching modes was found to be a challenge, and details of charge retention in components for both modes were experimentally measured and numerically modeled. Charge imbalance was found largely a result of liquid line size difference and condenser size difference. Modeling of void fraction in headers was noticed very important for good prediction of charge retention in microchannel heat exchangers.

1. INTRODUCTION

In recent years, electric vehicles have become increasingly popular. One key challenge that EV's are facing with is drive range anxiety. Most of the current Battery Electric Vehicles have a drive range of only around 100 miles per full charge. To make it worse, cabin climate control, especially cabin heating with resistance heater, can consume as much power as the drive train, and can cause the EV drive range to reduce up to 60%. While EV drive range can be increased by extending the battery pack to store more electric energy, the added cost is substantial. Lots of effort on reducing power consumption for cabin climate control has been carried out by researchers, mainly in three categories: reducing load, thermal storage, and reversible heat pump. This article is focused on heat pump for cabin heating.

Currently, there are a few EV models using heat pump for cabin heating, including Nissan Leaf, Renault Zoe, BMW i3, Kia Soul, and Volkswagen E-Golf, and this list is still growing. Roughly 20~30% drive range increase in cold weather was reported by using heat pump compared to using PTC heaters. Automotive heat pump systems has been investigated in open literature since 2000, when a transcritical CO_2 mobile heat pump prototype system was studied in the University of Illinois by Bullard et al. (2000). Numerous automotive suppliers have looked into different configurations of mobile heat pump systems, including Valeo (Hesse and Valeo, 2002, Benouali et al., 2012), Denso (Hunemorder et al., 2003), Visteon (Antonijevic and Heckt, 2004), Behr (Wawzyniak, 2012), Delphi (Kowsky et al., 2012), CTS (Musser and Hrnjak, 2014), etc. These system configurations range from direct air-to-refrigerant, indirect air-to-coolant-to-refrigerant, to different combinations of the two. Some of them also provide solutions to integrate thermal management of traction battery, power electronics and electric motor (PEEM).

This article studies the heat pump system from a Nissan Leaf EV, a compact electric car that has been available on the market for a few years. Details of the heating performance characteristics of this system has been studied by Feng and Hrnjak (2016), and some of those features will be revisited here. A numerical system model was built for future design purposes and was compared to the physical system. Charge imbalance when switching modes, details of charge retention in components, and modeling of charge retention were discussed.

2. EXPERIMENTAL FACILITY

The heat pump system was assembled with identical heat exchangers from a Nissan Leaf in the same configuration as was on an actual car. This system, as shown in Figure 1, consists of three heat exchangers: an evaporator provides cooling for the cabin in A/C mode, an inner condenser supplies heat in HP mode, and an outdoor heat exchanger to dissipate heat to the ambient as a condenser in A/C mode, while to harvest heat from outside air as an evaporator in HP mode. An open shaft compressor replaced the original electric compressor, with rotation speed adjusted to resemble the electric compressor. A transparent accumulator prevents excessive amount of liquid entering compressor suction chamber, and allows measurement of system charge demand variation under different operating conditions. Two electronic expansion valves (EEV) were installed instead of the original orifice tubes to explore control opportunities. Switching between different working modes were achieved by switching a three-way valve, a bypass valve, and an air side flap door upstream the inner condenser. The heat exchangers were installed inside wind tunnels and placed into environmental chambers, as shown in Figure 2. Thermocouples, pressure transducers, and flow meters were installed in air side and refrigerant side to determine heat exchanger capacities. With sensors properly calibrated, refrigerant side capacity can be measured within 3% of uncertainty when both inlet and outlet enthalpy measurement points are single phase, and air side capacities are determined with average uncertainty of about 4% for indoor evaporator, 6% for inner condenser, and 9% for outdoor heat exchanger. In order to study refrigerant charge distribution, extra ball valves and charging ports were installed so that quick close valve method can be employed to isolate refrigerant charge in components, and remove and weigh technique was then applied to extract and measure refrigerant charge retention in each component.

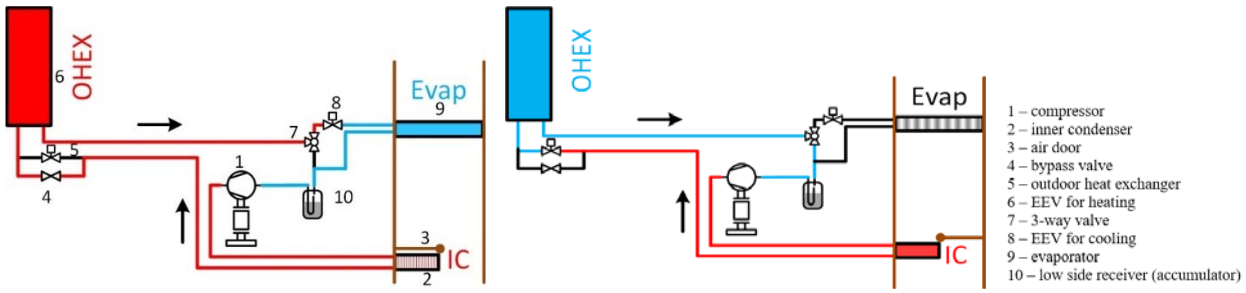

(a). A/C mode (b). HP mode

Figure 1. Reversible heat pump system configuration

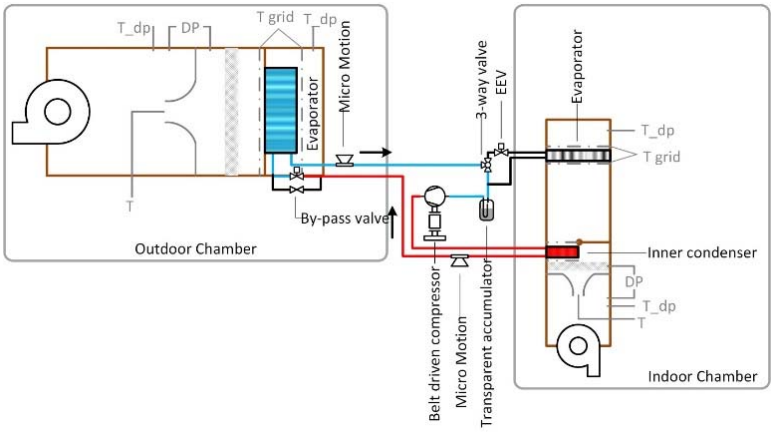

Figure 2. Testing facility

3. MODEL DEVELOPMENT

3.1 Compressor Model

Rasmussen and Jakobsen (2000) have categorized compressor models according to their level of physical details included, ranging from purely physical models with details of compressor structure to purely statistical models obtained solely from experimental data and contained no physical insights. In this study, experimental data for the

specific compressor from various operating conditions were available. Hence, the compressor model was generated by curve fitting based on some level of physical understandings. Compressor volumetric efficiency was correlated with compression ratio in equation (1), and clearance volume ratio ε_{cv} and compression polytropic exponent n_{poly} were found by curve fitting. The ratio of isentropic efficiency and volumetric efficiency was fitted with compression ratio in a linear form, as shown in equation (2). Considering heat loss from compressor shell, a constant thermal efficiency of 0.94 was assumed to relate thermal work and shaft work. Based on these three compressor efficiencies, from input of suction state, discharge pressure, and compressor speed, the model determines refrigerant mass flow rate, exit enthalpy, and shaft work. Since discharge pressure is physically at the outlet of the compressor, it should be iteratively solved in a system model.

$$\eta_{volm} = 1 - \varepsilon_{cv}\left[\left(\frac{P_{dis}}{P_{suc}}\right)^{1/n_{poly}} - 1\right] \tag{1}$$

$$\frac{\eta_{isen}}{\eta_{volm}} = 0.0327\frac{P_{dis}}{P_{suc}} + 0.5707 \tag{2}$$

3.2 Accumulator Model

The accumulator serves as a liquid-vapor separator before the compressor suction, while at the same time returns oil into compressor through a pinhole at the bottom of a suction U-tube. Apart from the fact that refrigerant can dissolve in oil, for most cases in HP mode, the accumulator always retains some excessive liquid refrigerant, primarily due to charge imbalance between A/C and HP modes. The liquid refrigerant is well mixed with oil, and will inevitably enter compressor suction chamber together with oil. The accumulator model was developed to determine suction quality based on derivation of liquid refrigerant mass flow rate through the pinhole. The liquid flow through the pinhole is driven by the pressure difference across it, which consists of four components: dynamic pressure difference, hydraulic pressure, frictional pressure loss from inlet side of the U-tube, and pressure loss from inlet restriction of the U-tube. The dynamic term is calculated with equation (4). The hydraulic term can be determined by using the liquid level with equation (5), while liquid level relies on the prediction of refrigerant charge retention in all components. The frictional term was calculated using Churchill (1977) correlation, as shown in equations (6) and (7). The inlet restriction term is usually the dominant pressure difference. Modeling of this term is based on experimental data. As measurements of pressure drop through the accumulator were available, frictional pressure loss was deducted from measurements to derive the inlet restriction term, and it's eventually fitted in equations (8) and (9) with a discharge coefficient linearly dependent on Reynolds number. With the driving pressure difference, liquid mass flow rate through pinhole is modeled with equation (10) as orifice flow, and suction quality with equation (11). The discharge coefficient for flow through the pinhole was taken as a constant of 0.68. The series of equations are solved iteratively to get suction quality since some pressure difference terms rely on this output quality.

$$\Delta P = \Delta P_{dyn} + \Delta P_{hyd} + \Delta P_{fri} + \Delta P_{res} \tag{3}$$

$$\Delta P_{dyn} = \frac{G_{Utube}^2}{2\rho_g} \tag{4}$$

$$\Delta P_{hyd} = \rho_f g h_{ll} \tag{5}$$

$$\Delta P_{fri} = f\frac{L}{D}\frac{G_{Utube}^2}{\rho_g} \tag{6}$$

$$A = \left[2.457\ln\left(\frac{1}{\left(7/\mathrm{Re}_D\right)^{0.9} + 0.27\left(\varepsilon/D\right)}\right)\right]^{16}$$

$$B = \left(\frac{37530}{\mathrm{Re}_D}\right)^{16} \tag{7}$$

$$f = 8\left[\left(\frac{8}{\mathrm{Re}_D}\right)^{12} + \left(A+B\right)^{-1.5}\right]^{\frac{1}{12}}$$

$$\Delta P_{res} = \frac{1}{C_{d,res}^2} \frac{G_{Utube}^2}{2\rho_g} \tag{8}$$

$$C_{d,res} = 0.94 - 3.5 \times 10^{-6} \, \mathrm{Re}_D \tag{9}$$

$$\dot{m}_{ref,liq} = C_{d,pinhole} A_{pinhole} \sqrt{2\Delta P \cdot \rho_f} \tag{10}$$

$$x_{cpri} = 1 - \frac{\dot{m}_{ref,liq}}{\dot{m}_{ref}} \tag{11}$$

3.3 Microchannel Heat Exchanger Model

All of the three heat exchangers used in the experimental system are microchannel type. They were modeled using finite volume method under the following assumptions:

1. Steady state flow and heat transfer;
2. Thermodynamic equilibrium, or otherwise noted;
3. Uniform distribution among parallel tubes, or otherwise noted;
4. Heat transfer and pressure drop in headers neglected;
5. Thermal resistance by conduction through tube wall neglected;
6. Lubricant effect not included in current study;
7. Dry condition.

Heat exchangers were first divided into refrigerant flow passes, and each pass was segmented into small elements along refrigerant flow direction. The number of elements per pass was determined by sensitivity analysis, to ensure heat exchanger capacity change to be less than 0.5% by doubling this number. Heat transfer coefficient on both refrigerant side and air side were then calculated using empirical correlations from the literature. Heat transfer amount was determined by using ε-NTU method. Meanwhile, pressure drop was calculated by empirical correlations according to element inlet states, and refrigerant mass retention were estimated using a void fraction correlation. The entire heat exchanger was solved element by element following refrigerant flow direction. For indoor evaporator and inner condenser, iteration was needed since these two heat exchangers had two slabs arranged in the opposite direction with air flow. Correlations used in the model are listed in Table 1.

Table 1. Correlations used in microchannel heat exchanger model

Fluid	Parameter	Correlation
Refrigerant (R134a)	Single phase HTC	Gnielinski (1976)
	Single phase frictional pressure drop	Churchill (1977)
	Two phase evaporating HTC	Kandlikar (2014)
	Two phase condensing HTC	Cavallini et al. (2006)
	Superheated condensing HTC	Kondou and Hrnjak (2012)
	Two phase evaporating frictional pressure drop	Friedel (1976)
	Two phase condensing frictional pressure drop	Cavallini et al. (2009)
	Two phase void fraction	Zivi 1964
Air	HTC	Chang and Wang 1996
	Pressure drop	Chang et al. (1994)

3.4 System Model

The system model connects all the component models in the same configuration as the physical system by using pressure and enthalpy as connecting parameters. Starting with the compressor, suction and discharge pressure are first initialized to reasonable guess values. Then refrigerant mass flow rate is obtained by the compressor model and send to other components as an input. From compressor model outlet state, following refrigerant flow direction, inner condenser model generates heating capacity and a certain level of subcooling. Compressor speed and discharge pressure are then adjusted to meet desired output heating capacity and subcooling. The expansion valve is modeled by an isenthalpic process. Outdoor heat exchanger inlet pressure is found such that its exit quality meets suction quality. Charge retention in components are then used as an input to accumulator model to generate suction quality and suction pressure, which update the guessed values at compressor inlet for next iteration. When the cycle converges, system performance parameters and refrigerant state variables can be returned as model outputs.

4. MODELING RESULTS AND DISCUSSION

4.1 Component Model Results

Figure 3 shows the comparison of modeled compressor output refrigerant mass flow rate and shaft work compared to experimental measurements. For most data points, refrigerant mass flow rates were well predicted, indicating good representation of the volumetric efficiency. However, compressor shaft work was in general underestimated for about 10%. The difficulty mainly comes from the two phase refrigerant inlet condition that prevails in the data for HP mode operations. The accumulator modeled suction quality and pressure drop are compared in Figure 4. Suction quality was reasonably represented by the model except for some conditions with very low ambient temperature or very low liquid level. In those situations, temperature effect on viscosity, or higher oil concentration in liquid retained in accumulator may strongly affect the model calculation, since no oil effect has been included. Estimation of pressure drop through the accumulator was on the conservative side, but in a reasonable range.

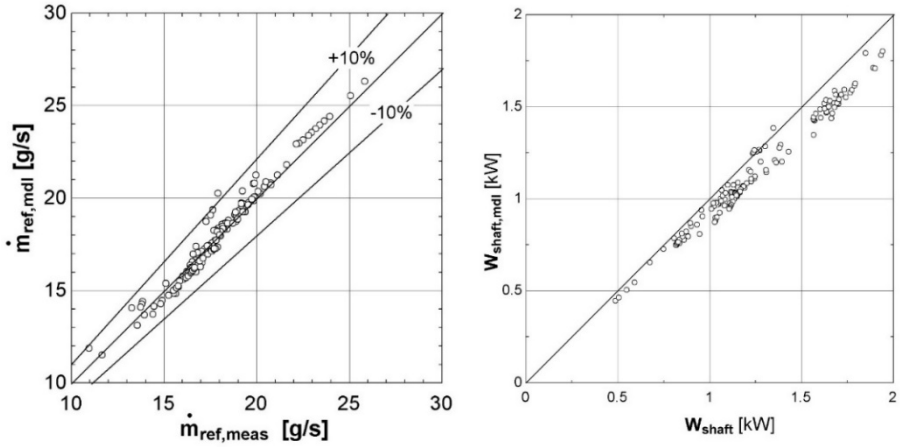

(a). Refrigerant mass flow rate (b). Compressor shaft work

Figure 3. Compressor model

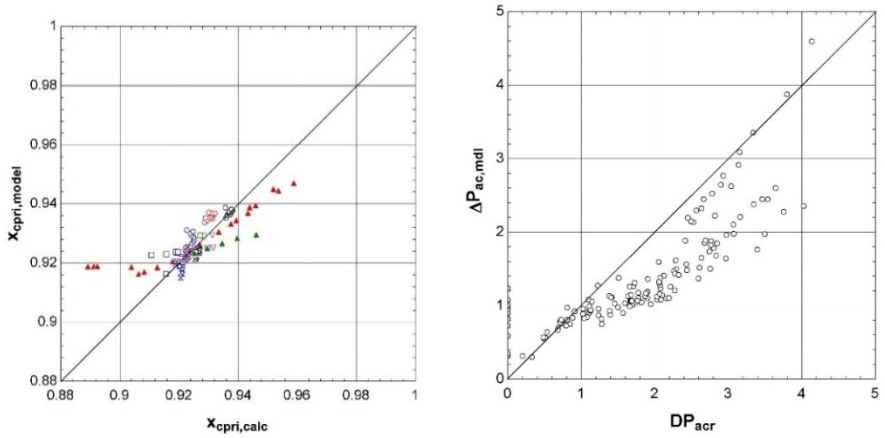

(a). Suction quality (b). Pressure loss through accumulator

Figure 4. Accumulator model

Heat exchanger models worked well in predicting heat transfer capacity of the evaporator, inner condenser, and outdoor heat exchanger as a condenser in A/C mode, as shown in Figure 5 (a), (b), (c). However, for outdoor heat exchanger working as an evaporator in HP mode, capacity was overestimated by an average of 16%, as shown in Figure 5 (d). Figure 5 (e) shows a picture of the frost formation at outdoor heat exchanger surface when the system has been running for a while in HP mode in a humid cold ambient. The frost pattern acts as an indication of transition from two phase to superheated state of the interior refrigerant flow. From the photograph, the frosted length at the second flow pass varies dramatically from tube to tube, indicating severe maldistribution of two phase refrigerant flow. As superheated region has much lower refrigerant side heat transfer coefficient and smaller air-to-refrigerant

temperatue difference, the heat transfer ability in this region was largely deteriorated. By using the frosted length profile from the photo as liquid mass flow rate distribution profile into parallel microchannel tubes, and iteratively solve vapor mass flow rate distribution to ensure identical outlet pressure from different flow pathes, heat exchanger capacity can be determined for the maldistribution case. With this approach, outdoor heat exchanger capacities were recalculated with input from the frost photo, shown in Figure 5 (d). Compared to the results obtained with uniform distribution assumption, this approach turns out more reasonable. Nevertheless, the frost pattern is only an indirect measure of maldistribution at only one operating condition. Further study is needed to generalize the effect of maldistribution on heat exchanger and system performance under different conditions. Figure 5 (f) shows the modeled outdoor heat exchanger surface temperature with the above described approach. With the aid of surface temperature measurement like an infrared image, this model could be used to look into details of refrigerant maldistribution.

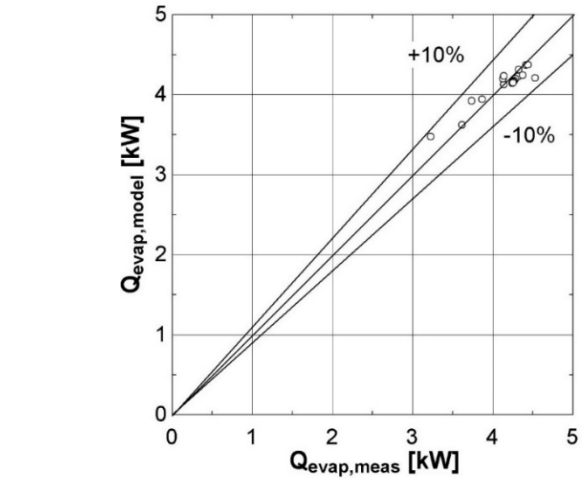

(a). Evaporator

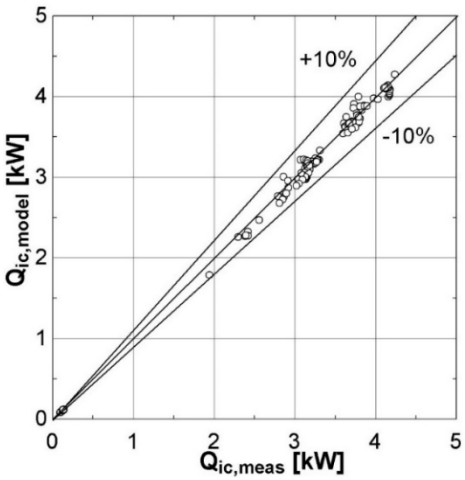

(b). Inner condenser

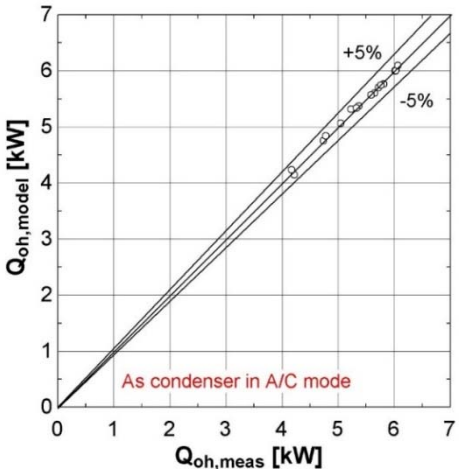

(c). OHEX as a condenser

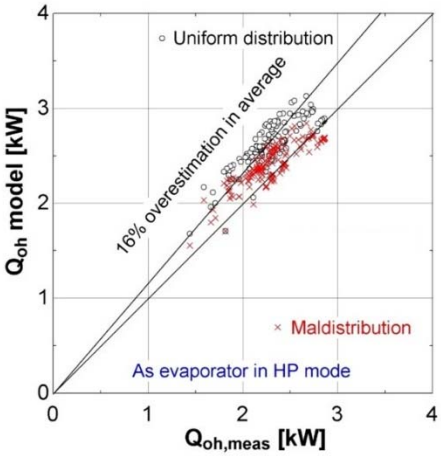

(d). OHEX as an evaporator

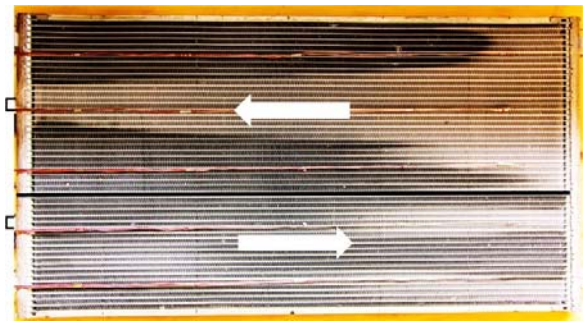

(e). Frost photo indicates severe maldistribution

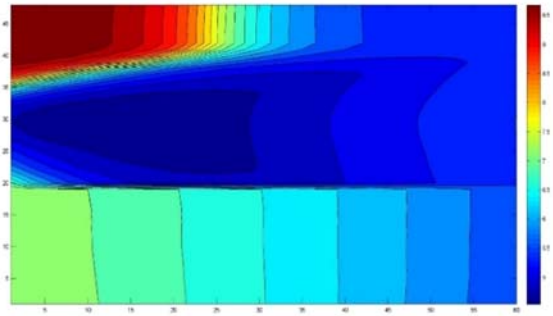

(f). Modeled heat exchanger surface temperature

Figure 5. Heat exchanger model

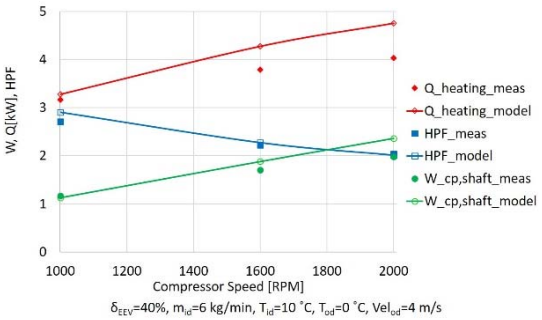

(a). Effect of compressor speed

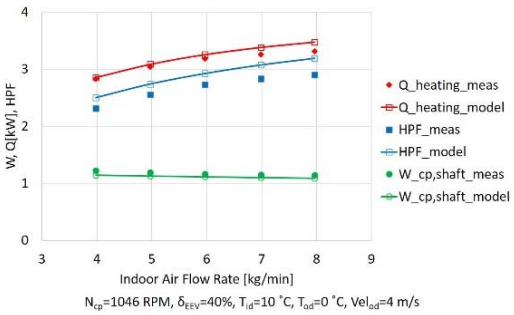

(b). Effect of indoor air mass flow rate

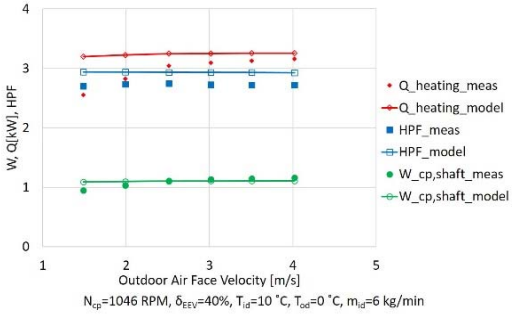

(c). Effect of outdoor air face velocity

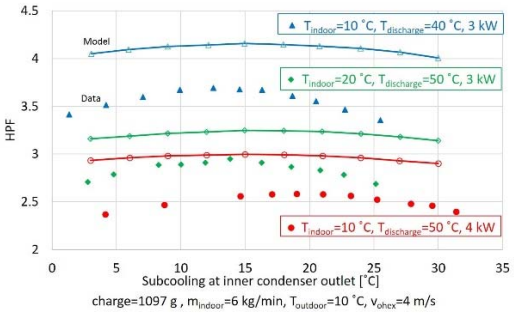

(d). Maximizing HPF by controlling subcooling

Figure 6. System model results

4.2 System Model Results

System modeling was carried out for four series of cases in HP mode, using input variables of system refrigerant charge, indoor and outdoor air temperature and flow rates, compressor speed or target air discharge temperature, and subcooling. Note that subcooling is required as an input by the system model due to the lack of a flow equation for the expansion device. Model output system performance variables of compressor shaft work, heating capacity, and HPF were compared with experimental data. As shown in Figure 6, the modeled system responses to changing compressor speed and indoor air flow rate matches with the experimental responses quite well. For changing compressor speed, both heating capacity and shaft work were overestimated, while HPF was well predicted, indicating the model was too optimistic on the outdoor heat exchanger. Implementing maldistribution effect into the system model should improve performance prediction. For changing indoor air mass flow rate, the aforementioned under prediction of shaft work, together with neglecting of maldistribution, caused the HPF to be overestimated. Modeled system response to outdoor air face velocity, however, differs from the physical system. The real system heating capacity increased about 20% by increasing outdoor air face velocity from 1.5 to 3 m/s, while the modeled system is rather insensitive to face velocity. Possible reasons for this difference can be overestimation of air side heat transfer coefficient at low air flow rate, or the physical system experiences more severe maldistribution when air flow rate is lower. Figure 6 (d) shows the HPF variation for different levels of subcooling at three different operating conditions. The experimental data shows about 10% variation of HPF by controlling subcooling while heating capacity was maintained by adjusting compressor speed, a feature useful for energy efficiency optimization. The modeled system shows maximum HPF at subcooling level of 15 °C, quite close to the experimentally determined optimum for each condition, however, the variation of HPF were only about 4%, and the values of modeled HPF were 10~20% higher than experimental measurements.

5. CHARGE IMBALANCE AND RETENTION

From the charge determination tests carried out for both A/C and HP modes, the system refrigerant charge demand at A/C mode was found about 300 g greater than that needed for HP mode, as shown in Figure 7. By using quick close valve technique to isolate refrigerant in components, charge retention in components were determined for both A/C and HP modes at certain working conditions, as shown in Figure 8. The inner circle represents the internal volumes of components and connecting tubes, and the outer circle indicates the amount of refrigerant retained in the corresponding components. It was noticed that the liquid lines for both modes has a large internal volume, and the

line size difference caused about 150 g of charge imbalance. The majority of the rest charge imbalance was largely caused by the condenser size difference when switching modes. The system model developed in the previous sections offers an opportunity to look into more details of charge distribution. With the simple charge model of using only Zivi (1964) void fraction correlation for all two-phase regions, including headers and microchannel tubes, the model gave retention results shown in Table 2. Compared to experimentally extracted charge amount, the model underestimated charge retention for all three heat exchangers in both modes. Further divide the heat exchangers into microchannel tubes and headers, it was noticed that headers occupies the majority of heat exchanger internal volume, as listed in Table 3. Hence accuracy of prediction of charge retention in headers is critical. Zivi (1964) correlation was developed based on annular flow regime. For two phase flow in microchannels, slug flow and annular flow are the dominant flow regimes, and Zivi (1964) correlation is reasonably applicable for most situations for the three heat exchangers studied. For flow in headers, however, with larger cross-sectional area and large variation of mass flow rate due to flow branching in or out, the mass flux inside headers varies greatly, while very different flow regimes can occur. As Zivi (1964) correlation didn't take into account of mass flux, it is not appropriate to be used in headers. Details of void fraction and charge retention in outdoor heat exchanger headers was explored by applying the flow regime map developed by Hewitt and Roberts (1969) for vertical upward flow, and a selection of void fraction correlations according to the flow regimes. With this preliminary approach, charge retention prediction results become more reasonable. Due to the complex nature of two phase flow in headers, much more research effort is needed in order to accurately model void fraction in headers and charge retention in microchannel heat exchangers.

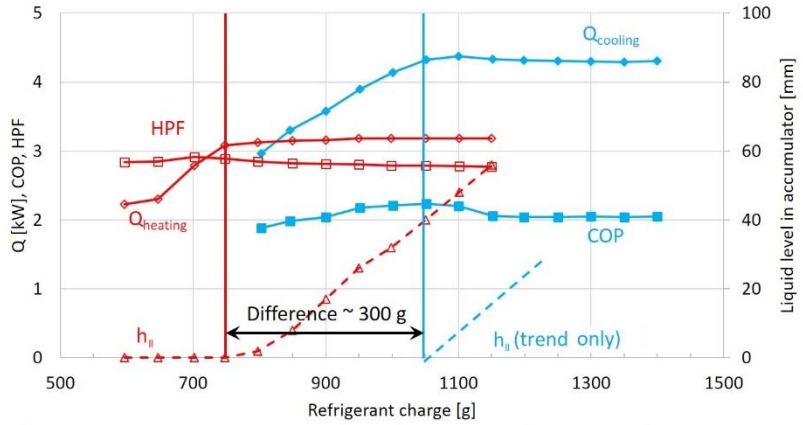

Figure 7. Charge requirement for A/C and HP modes differs largely

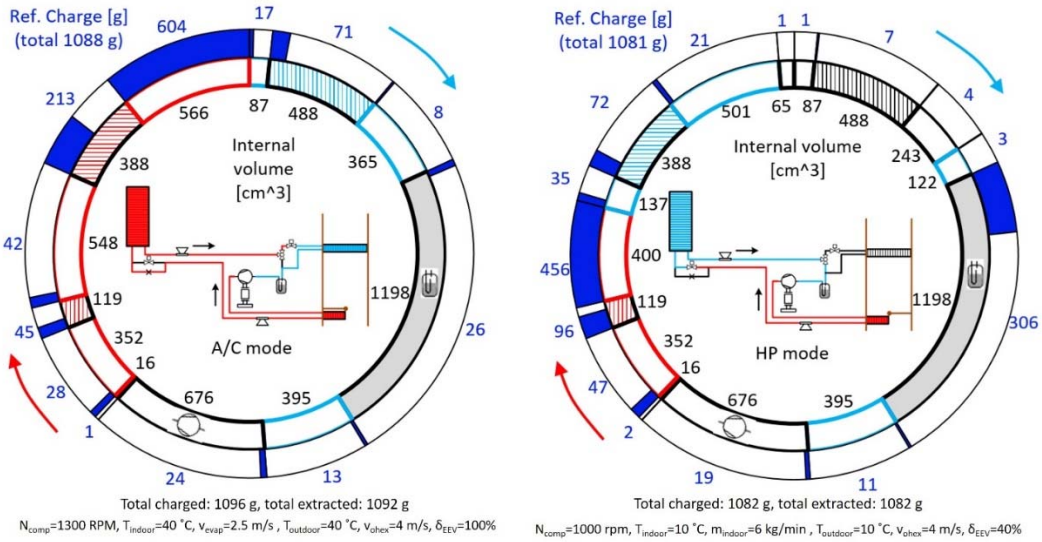

Figure 8. Refrigerant charge retention in components

Table 2. Refrigerant charge retention in components

m_{ref} [g]	A/C mode				HP mode			
	OHEX	Evap	IC	Total	OHEX	Evap	IC	Total
Measured	213	71	45	329	72	7	96	175
Modeled (Zivi 1964)	170	49	7	226	37	6.8	71	115
Microchannel tubes (modeled)	*78*	*17*	*4*	*99*	*16*	*2.4*	*37*	*55*
Headers (modeled)	*92*	*32*	*3*	*127*	*21*	*4.4*	*34*	*60*
Modeled (flow regime map based)	186	-	-	-	70	-	-	-

Table 3. Internal volume of microchannel tubes and headers of all three heat exchangers

V [cm^3]	OHEX	Evap	IC
MC tubes	180	173	61
Headers	308	315	58

6. CONCLUSIONS

A numerical model for a mobile reversible heat pump system was built and presented. Component wise, the compressor model and accumulator fairly represented the physical components, while compressor shaft work was slightly underestimated, possibly due to insufficient consideration of two phase inlet to suction chamber. Heat exchanger models worked well to predict heat transfer capacity for the evaporator, inner condenser, and outdoor heat exchanger as a condenser in A/C mode. However, capacity prediction for outdoor heat exchanger as an evaporator in HP mode was overestimated by an average of 16%. By invoking the not included maldistribution effect, using an externally measured frost pattern as input for liquid mass flow rate distribution in parallel channels, the capacity prediction was improved. Generalization of maldistribution and its effect on heat exchanger and system performance needs further study. System wise, when component models were connected as a system model, heating performance characteristics with changing compressor speed and indoor air mass flow rate matched well with experimental findings. The modeled system was not as sensitive to outdoor air flow rate as the physical setup. HPF of the modeled system varies about 4% by controlling subcooling for fixed capacity, compared to about 10% variation of the experimental measurement, and the values of HPF were overestimated by 10~20%. As switching modes can lead to system charge imbalance of up to 300 g, the model also looked into charge retention in both modes. It was identified that headers have major contribution in retaining charge, and flow situation in headers can vary largely. Much more details of void fraction in headers need to be addressed in order to predict charge retention in microchannel heat exchangers, and to help design system with minimal charge imbalance when switching modes.

NOMENCLATURE

A/C	air conditioning
COP	coefficient of performance, $Q_{cooling}/W_{cp,shaft}$
EEV	electronic expansion valve
EV	electric vehicle
HP	heat pump
HPF	heating performance factor, $Q_{heating}/W_{cp,shaft}$
HTC	heat transfer coefficient
ICE	internal combustion engine
PEEM	power electronics and electronic motor
PTC	positive temperature coefficient
SC	subcooling
SH	superheat
ac	accumulator
cp	compressor
e, evap	evaporator
ic	inner condenser
oh, ohex	outdoor heat exchanger
dis	discharge
suc	suction
a/r	air side/refrigerant side
i/o	inlet/outlet
f	liquid phase
g	gas phase/gravitational acceleration
dyn	dynamic term
fri	frictional term
hyd	hydraulic term
res	inlet restriction term
id/od	indoor/outdoor
$\mathbf{h_{ll}}$	liquid level
T	temperature
P	pressure
x	vapor quality
$\mathbf{n_{poly}}$	polytropic exponent
$\boldsymbol{\delta_{EEV}}$	EEV opening size
$\boldsymbol{\varepsilon_{cv}}$	clearance volume ratio
$\boldsymbol{\eta_{volm}}$	volumetric efficiency
$\boldsymbol{\eta_{isen}}$	isentropic efficiency

REFERENCES

Antonijevic, D., Heckt, R., (2004). Heat pump supplemental heating system for motor vehicles. *Proc Instn Mech Engrs*, Vol. 218, Part D, 1111-1115.

Benouali, J., Gardie, P., Beauvis, R., Delaforge, L., Porto, M., Petitjean, C., (2012). Heat pump architectures for electrified cars. *SAE 2012 World Congress*, presentation 12TMS-0001.

Bergman, T.L., Lavine, A.S., Incropera, F.P., Dewitt, D.P., (2011). Fundamentals of Heat and Mass Transfer, 7th Ed.. John Wiley & Sons.

Bullard, C.W., Yin, J.M., Hrnjak, P.S., (2000). Transcritical CO_2 mobile heat pump and A/C system experimental and model results. *SAE 2000 World Congress*, presentation.

Cavallini, A., Del Col, D., Matkovic, M., Rossetto, L., (2009). Frictional pressure drop during vapour–liquid flow in minichannels: Modelling and experimental evaluation. *Int. J. of Heat Transfer and Fluid Flow*, 30(1), 131-139.

Cavallini, A., Doretti, L., Matkovic, M., Rossetto, L., (2006). Update on Condensation Heat Transfer and Pressure Drop inside Minichannels. *Heat Transfer Engineering*, 27(4), 74-87.

Chang, Y., Wang, C. and Chang, W., (1994). Heat Transfer and Flow Characteristics of Automotive Brazed Aluminum Heat Exchangers. *ASHRAE Trans.*, 100(2), 643-652.

Chang, Y.J., Wang, C.C., (1996). Air Side Performance of Brazed Aluminum Heat Exchangers. *J. of Enhanced Heat Transfer*, 3(1).

Chang, Y.J., Wang, C.C., (1997). A Generalized Heat Transfer Correlation for Louver Fin Geometry. *Int. J. of Heat and Mass Transfer*, 40(3), 533-544.

Chen, J.C., (1963). A correlation for boiling heat transfer to saturated fluids in convective flow. *ASME Paper*, 63-HT-34 (1963) 1-11.

Churchill, S.W., (1977). Friction-factor equation spans all fluid-flow regimes. *Chemical Engineering*, 84(24), 91-92.

Feng, L. and Hrnjak, P., (2016). Experimental Study of an Air Conditioning-Heat Pump System for Electric Vehicles. *SAE Int. J. Passeng. Cars - Mech. Syst.* 9(1):2016, doi:10.4271/2016-01-0261.

Hesse, U., Valeo, Z., (2002). Results from CO2 heat pump applications. *SAE 2000 Automotive Alternative Refrigerant Systems Symposium*, presentation.

Hunemorder, W., Kakehashi, N., Inui, K., (2003). CO_2 heat pump with electrical compressor. *VDA Alternative Refrigerant Winter Meeting*, presentation.

Kandlikar, S.G., Garimella, S., Li, D., Colin, S., King, M.R., (2014). Heat Transfer and Fluid Flow in Minichannels and Microchannels, 2nd Ed.. Elsevier.

Kondo, C., Hrnjak, P.S., (2012). Heat Rejection in Condensers: Desuperheating, Condensation in Superheated Region and Two Phase Zone. *Int. Refrigeration and Air Conditioning Conf.*

Kowsky, C., Wolfe, E., Leitzel, L. and Oddi, F., (2012). Unitary HPAC System. *SAE Int. J. Passeng. Cars - Mech.Syst.* 5(2):2012, doi:10.4271/2012-01-1050.

Musser, A. and Hrnjak, P. S., (2014). Mobile Heat Pump Exploration Using R445A and R744. *International Refrigeration and Air Conditioning Conference*. Paper 1514.

Rasmussen, B.D., Jakobsen, A., (2000). Review of Compressor Models and Performance Characterizing Variables. *International Compressor Engineering Conference*. Paper 1429.

Rennels, D.C., Hudson, H.M., (2012). *Pipe Flow: A Practical and Comprehensive Guide, 1st Ed.*. John Wiley & Sons.

Thome, J.R., (2004). Engineering Data Book III. Wolverine Tube, Inc.

Wawzyniak, M., (2011). Benefits and challenges of heat pump systems. *SAE 2011 Alternative Refrigerant Systems Symposium*, presentation 11AAR-0009.

ACKNOWLEDGEMENT

This work was supported by the Air Conditioning and Refrigeration Center at the University of Illinois at Urbana-Champaign. All help from center members and sponsor companies are gratefully acknowledged!